J Mater Sci: Mater Electron (2012) 23:2276–2281
DOI 10.1007/s10854-012-0816-4

Tunable morphology and optical absorption of bismuth ferrite synthesized by sol–gel–hydrothermal method

Yi Liu · Ruzhong Zuo

Received: 28 April 2012 / Accepted: 24 June 2012 / Published online: 30 June 2012

Abstract Bismuth ferrite $BiFeO_3$ (BFO) powders with various morphologies were successfully prepared via a sol–gel–hydrothermal synthesis process. The as-prepared samples were characterized by X-ray diffraction, scanning electron microscopy and energy dispersive spectroscopy. Microspheres and microcubes were obtained as Bi–Fe–glycerol sol was used as precursor, and submicrometer-sized particles could be prepared by using Bi–Fe–glycerol gel. Possible formation mechanism of BFO microcrystals was proposed in this work. Moreover, the results of UV–vis diffuse reflectance spectroscopy reveal that BFO powders can be used as an effective photocatalyst under visible light in addition to its ferroelectric and magnetic applications.

1 Introduction

Perovskite-type bismuth ferrite $BiFeO_3$ (BFO), possess a rhombohedrally distorted perovskite structure with the space group R3c at room temperature [1, 2]. The coexistence of ferroelectricity (FE) and antiferromagnetic (AFM) ordering at room temperature makes this material be one of the most promising candidates for room-temperature magnetoelectric applications [2–4]. More and more attention has been paid to the BFO material since its thin films have made great achievements.[3] In addition to the potential magnetoelectric applications, BFO is also an important photocatalystic material in visible light region owing to its narrow band-gap energy ($\sim$2.18 eV) and high chemical stability [5–8]. However, it is very difficult to fabricate bulk BFO with the absence of nonferroelectric impurities such as $Bi_2Fe_4O_9$ and $Bi_{25}FeO_{40}$ through conventional solid-state reaction. In the solid-state route, nitric acid leaching is necessary to eliminate the impurity phases, which results in coarser powders and poor reproducibility. Most recently, a successful method named "rapid liquid sintering" with an equimolar mixture of precursor oxide reactants has been reported [4].

In order to overcome these disadvantages, various wet chemical methods have been applied to synthesize pure-phase BFO powders, such as co-precipitation [9], microemulsion method [10], ferrioxalate precursor process [11], sol–gel method [12–15], and hydrothermal synthesis [16–27]. Pure-phase BFO powder has been successfully prepared by sol–gel methods based on a variety of routes, such as citric acid route [12], ethylene glycol route [14, 28], glycerol route [15] and so on [13, 29]; however, a further calcination step at higher temperature (>400 °C) is still required, which also results in the agglomeration, irregular morphology, broad distribution of the particle size, and the bismuth volatilization of BFO powders. In contract, hydrothermal synthesis has been regarded as one promising method to produce fine ceramic powders with high crystallinity, high purity, high homogeneity, narrow particle size distribution, and controllable microstructure in a closed system under low temperature and high pressure. Currently, BFO with desirable morphologies, such as submicrometer-sized spindles [16], nanoparticles [18, 19], nanowires [21], microplates [22], microcubes and microspheres [23], polyhedral particles [24], nanoflakes [25], nanoparticles-assembled microrods [26], pills and rods [27], and flower-like particles [30] have been synthesized via hydrothermal and solvothermal routes. As a novel method to prepare oxide powders at moderate conditions,

Y. Liu · R. Zuo (✉)
Institute of Electro Ceramics and Devices, School of Materials Science and Engineering, Hefei University of Technology, Hefei 230009, People's Republic of China
e-mail: piezolab@hfut.edu.cn

the sol–gel–hydrothermal technique offers double advantages of both sol–gel and hydrothermal synthesis and has become attractive in the last decades. Bi-based complex perovskite nanowires, such as $Na_{0.5}Bi_{0.5}TiO_3$ [31], $K_{0.5}Bi_{0.5}TiO_3$ [32], $(Na_{0.8}K_{0.2})_{0.5}Bi_{0.5}TiO_3$ [33], and $(K_{0.5}Bi_{0.5})_{0.4}Ba_{0.6}TiO_3$ systems [34], $MnTiO_3$ particles [35] and $PbTiO_3$ microspheres [36] have been successfully obtained via a sol–gel–hydrothermal process.

In the present study, the sol–gel–hydrothermal process was attempted for the first time to prepare phase-pure BFO powders with various morphologies. Micrometer-sized spheres and cubes, submicrometer-sized BFO particles, have been successfully synthesized by controlling the hydrothermal conditions or changing the precursor. Possible formation mechanism for BFO microcrystals was also carefully discussed.

2 Experimental

The raw materials used in this study were bismuth nitrate ($Bi(NO_3)_3{\cdot}5H_2O$), iron nitrate ($Fe(NO_3)_3{\cdot}9H_2O$), potassium hydroxide (KOH), glycerol, and nitric acid. All chemicals were analytical grade purity and used as received without further purification. Firstly, equimolar amounts of $Bi(NO_3)_3{\cdot}5H_2O$ and $Fe(NO_3)_3{\cdot}9H_2O$ were dissolved in diluted HNO_3 to form aqueous solutions. Then, glycerol was introduced into the above Bi–Fe solution being stirred at 80 °C. The mol ratio of metal ion to hydroxyl groups in glycerol (M/-OH) was 1:1.5. As water was evaporated from the mixture solution, an orange Bi–Fe–glycerol sol was formed, accompanied by the evolution of NO_x gas resulting from the decomposition of nitrate ions. Upon continuously heating at 80 °C to remove the water, the Bi–Fe–glycerol sol becomes more viscous and then changes into a dried gel. The Bi–Fe–glycerol sol and dried gel were used as the precursor for further hydrothermal synthesis, respectively. A certain amount of KOH solution, which served as a mineralizer, was added to the Bi–Fe–glycerol sol (or dried gel). After being stirred for 30 min, the reaction mixture was transferred to a stainless steel Teflon-lined autoclave and heated at 200 °C under an auto-generated pressure for 24 h. After the end of the reaction, the autoclave was cooled to room temperature naturally, and the products were collected using a centrifuge and then washed with water and ethanol several times. Finally, the samples were dried at 70 °C for 6 h.

The products were analyzed by an X-ray diffractometer (XRD, D/Max-RB, Rigaku, Japan), in a 2θ range from 20° to 70°, using Cu Kα radiation. The morphology of the particles was observed using a field emission scanning electron microscopy (FE-SEM, Sirion200, FEI, USA) equipped with an energy-dispersive X-ray spectrometer (EDX). UV–vis diffuse reflectance spectra (DRS) of the samples were measured using barium sulfate as a standard material by a UV–vis spectrophotometer (TU-1950, Beijing Perkinje General Instrument Co., Ltd, Beijing, China) with an integrating sphere.

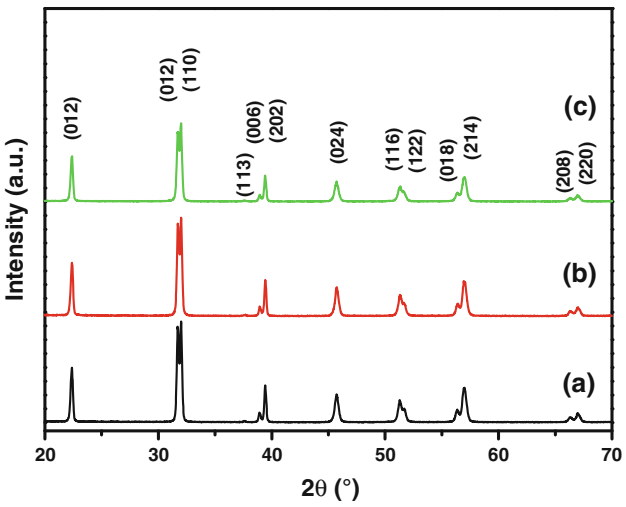

Fig. 1 XRD patterns of the as-synthesized samples under different hydrothermal conditions: **a** Bi–Fe–glycerol sol, 11 M KOH, 200 °C, **b** Bi–Fe–glycerol sol, 13 M KOH, 200 °C and **c** dried gel, 10 M KOH, 200 °C

3 Results and discussion

Figure 1 shows the XRD patterns of the products synthesized under different conditions. It can be seen that all the diffraction peaks in these patterns can be perfectly assigned to a pure-phase BFO (JCPDS No. 71-2494, space group: R3c), with a rhombohedrally distorted perovskite structure. The lattice constants calculated from the XRD data are presented in Table 1, which are well consistent with the literature values of a = b = 5.588 Å, and c = 13.867 Å (JCPDS No. 71-2494). No noticeable peaks from impurity phases were detected, demonstrating that single-phase and well crystallized BFO has been successfully prepared under current hydrothermal conditions.

The SEM images of the final products obtained by the hydrothermal process at 200 °C for 24 h from Bi–Fe–glycerol sol are shown in Fig. 2a, b. It is evident that the particle morphology and size of as-prepared BFO samples strongly depend on the KOH concentration. As shown in Fig. 2a, BFO microspheres with a diameter of ~5 μm were obtained as the KOH concentration was controlled at 11 M. EDX analysis performed on individual microsphere revealed that its chemical composition conforms to Bi/Fe atomic ratio of ~1.09:1 (Fig. 2c). When KOH concentration is 13 M, the as-prepared BFO has a cubic morphology and size of 2.5 μm (Fig. 2b). EDX performed on individual

Table 1 The effect of hydrothermal synthesis conditions on lattice constants, morphology, size and optical properties of BFO particles

Precursor	KOH concentration (M)	Lattice constants(Å)		Morphology	Particles size	Band gap (eV)
		a = b	c			
Bi–Fe–glycerol sol	11	5.580	13.847	Microspheres	5 μm	2.05
Bi–Fe–glycerol sol	13	5.580	13.840	Microcubes	2.5 μm	2.02
Dried gel	10	5.579	13.845	Submicrometer -sized particles	700 nm	2.10

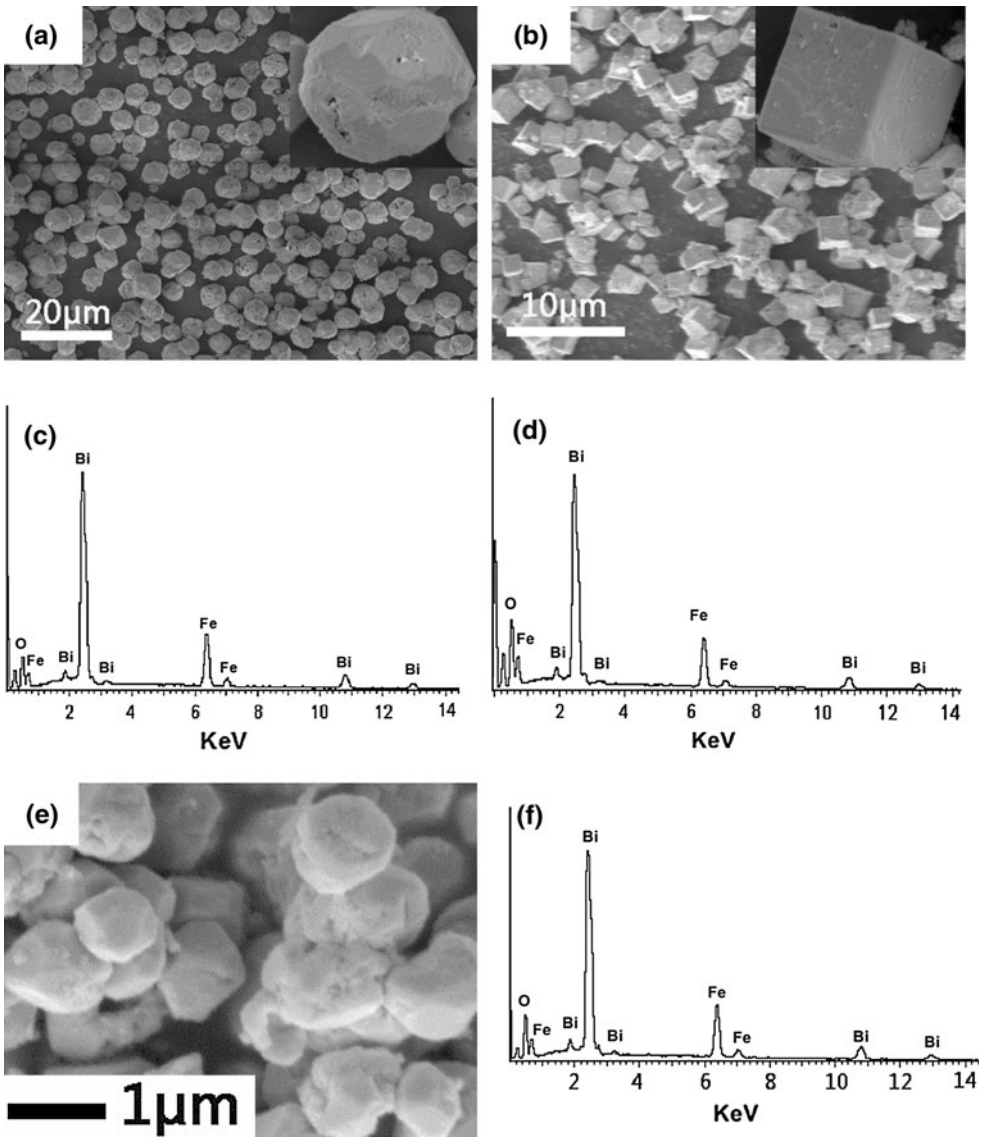

Fig. 2 SEM images of BFO powders synthesized from Bi–Fe–glycerol sol at 200 °C for 24 h under different KOH concentration: **a** 11 M and **b** 13 M; EDX patterns of BFO powders obtained from Bi–Fe–glycerol sol at different KOH concentration: **c** 11 M and **d** 13 M; **e** the SEM image of BFO particles synthesized from dried Bi–Fe–glycerol gel at 200 °C for 24 h under 10 M KOH; **f** EDX pattern of BFO particles from dried Bi–Fe–glycerol gel at 10 M KOH

BFO microcube (Fig. 2d) revealed that the atomic ratio of Bi/Fe is about 1.07:1, which is close to 1:1. The insets of Fig. 2a, b show the magnified images of microsphere and microcube. By using the dried gel instead of the Bi–Fe–glycerol sol as precursor, only submicrometer-sized particles were obtained as the KOH concentration was controlled at 10 M, as shown in Fig. 2e. The particle size evaluated from the SEM image approximates to 700 nm. The result of EDX analysis performed on submicrometer-sized particles (Fig. 2f) shows that the Bi/Fe molar ratio is 0.997:1. The effect of synthesis conditions on the morphology and particle size of as-prepared samples are summarized in Table 1. It can be concluded that, in addition to the KOH concentration, the difference of as-used

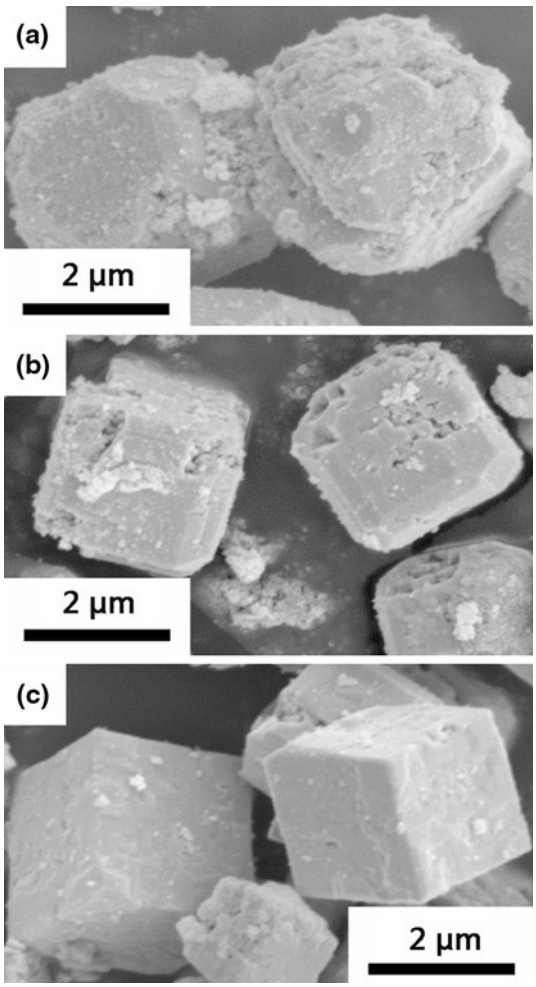

Fig. 3 SEM images of the BFO samples after **a** 3 h, **b** 6 h and **c** 24 h-hydrothermal treatment with 13 M KOH

precursor has an obvious effect on the final products in the hydrothermal process.

To clarify the formation mechanism, the BFO particles with cubic-shape morphology were taken as an example, so a series of experiments with varying reaction time were carried out, which corresponds to different stages of the hydrothermal reaction. Figure 3 shows the SEM morphology of the products at each stage. After a 3 h-hydrothermal treatment, crystallites with irregular shape and relatively rough surfaces (Fig. 3a) were obtained. After the reaction time was prolonged up to 6 h, rough and irregular crystallites start to transform into cubic particles with rough surfaces (Fig. 3b). Additionally, truncated faces could be found on the corner of the microcubes. As the reaction was extended to 24 h, the products became high-quality cubic-shape particles with more flat surfaces. Based on the evolution process of time-dependent particle morphology, we proposed that BFO microcrystal growth should take place through a dissolution/recrystallization mechanism. The nucleation and then growth process was predominant during the initial stage of hydrothermal process. At this stage, a large number of small BFO crystallites were produced. To minimize the overall energy of the system, a great number of primary particulates tend to agglomerate into loosely aggregated particles [37]. The recrystallization could happen at the solid–liquid interface between the aggregates and KOH solutions due to the mineralization effects of KOH. As the hydrothermal reaction continued, these loosely aggregated particles transformed into compacted agglomerates with rough surfaces, because the attached particulates grow up gradually at the expense of the newly produced primary particulates and smaller ones. Additionally, the surfaces of the cubes were smoothed by the conventional Ostwald ripening as well. It is known that the size and morphology of the final products strongly depend on both crystal nucleation and crystal growth [16]. The nucleation and growth rate depend on the degree of super-saturation, which is usually determined by OH^- concentration in the precursor solution. There would be a low nucleation rate and high growth rate at a low super-saturation, while a high nucleation rate and low growth rate will appear at a high super-saturation. Additionally, OH^- concentration plays a critical role in the process of dissolution–recrystallization. It has been supposed that OH^- ions were adsorbed on certain faces of oxide crystals, which may create additional growth anisotropy and modify the growth habit of crystals [38]. At a lower concentration of OH^- (11 M KOH), the adsorption of OH^- ions cannot change the growth habit of the agglomerates. These agglomerates with rough surfaces grow into spheres without obvious shape change. With the increase of OH^- concentration, the effect of OH^- ions was stronger. At a higher OH^- concentration (13 M KOH), the growth habit, that is the relative growth rates in different directions, was changed because of the stronger adsorption of OH^- ions, such that cubic-shape particles were formed. According the symmetries of pervoskite BFO and other relevant works

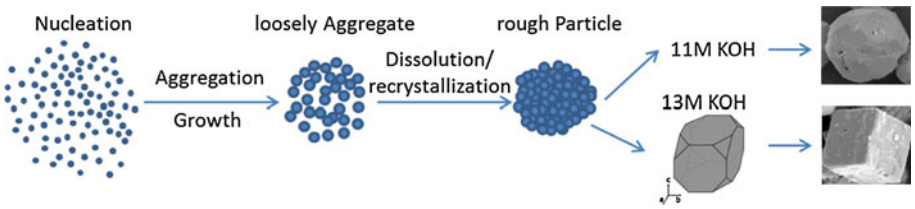

Fig. 4 Schematic illustration of the formation process of BFO microcrystals during hydrothermal process

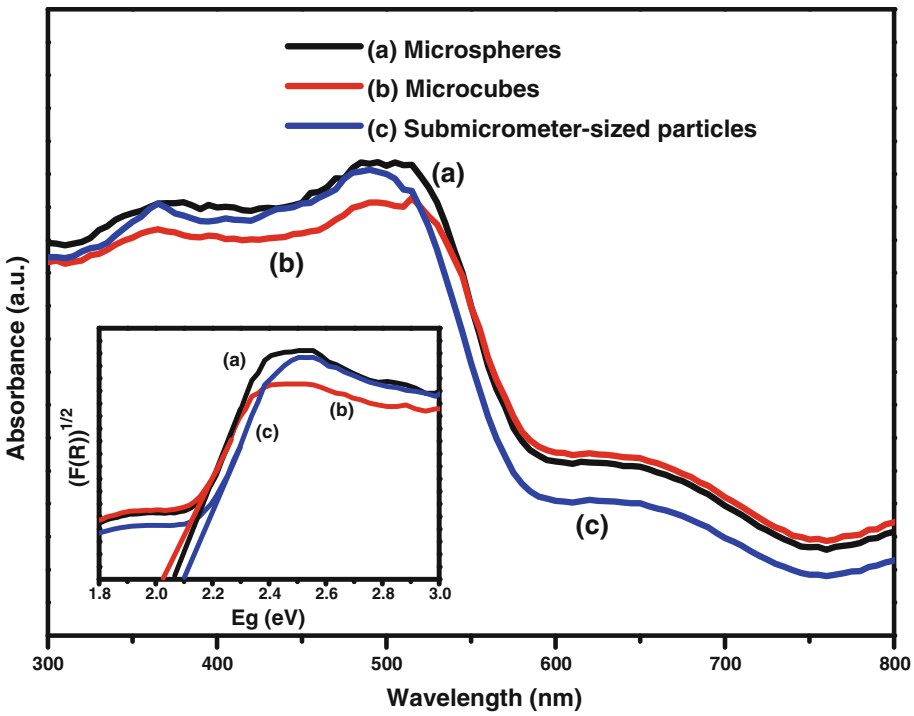

Fig. 5 UV–vis diffuse reflectance spectra of various BFO samples: **a** microspheres, **b** microcubes, and **c** submicrometer-sized particles; inset is the square root of Kubelka–Munk functions F(R) versus photo energy

[27, 39], the microcubes are most possibly enclosed with $\{100\}_c$ crystal faces. It has been suggested that the growth rate of the BFO microcrystals along <100> is lower than that along <111> [24]. As a result, the $\{100\}_c$ crystal faces were kept in the final morphology of BFO microcrystals, while the $\{111\}_c$ faces disappeared, which can be evidenced by the truncated faces observed in Fig. 3b and vanished in Fig. 3c. The formation process was illustrated in Fig 4. In addition, it can be found that the as-prepared microcubes ($\sim$2.5 μm) are smaller than BFO microspheres ($\sim$5 μm), which could be attributed to the increase in the nucleation and the degradation in the crystal growth rate with increasing OH^- concentration. Submicrometer-sized BFO particles were obtained when Bi–Fe–glycerol gel was used as precursor, which may be due to the stable complexes formed in the gel [15]. Glycerol has three hydroxyl groups and it can form complexes with metal ions (e.g., Bi^{3+} and Fe^{3+}). Then, the metal ions will be released slowly during hydrothermal reaction [40]. This may contribute to a decrease in both growth rate and agglomeration degree, and results in a smaller particle size.

It is of interest to explore the optical absorption property of the BFO particles because the UV–vis absorption is relevant to the electronic structure feature and the energy band of semiconductor catalyst. Figure 5 shows the absorption spectra of the as-prepared BFO products transformed from the corresponding diffuse spectra according to the well-known Kubelka–Munk (K-M) theory [41]. A broad absorption band in the range of 410–570 nm are observed in the absorption spectra, which indicates that all BFO samples can absorb considerable amounts of visible light in this range. This absorption region could be attributed to the result of two types of excitations overlapped with each other [42, 43]. The first excitation process is due to the pair excitation processes $^6A_{1g} + {}^6A_{1g} \rightarrow {}^4T_{1g}\ (^4G) + {}^4T_{1g}\ (^4G)$ and the second one is due to the excitation from $^6A_1$ to ^4E, $^4A_1\ (^4G)$ ligand field transitions and the charge-transfer band tail. The energy bandgaps of the BFO samples can be calculated from the tangent lines in the plot of the square root of K-M functions F(R) against photo energy [44], as shown in the inset of Fig. 5. As the tangent lines are extrapolated to $(F(R))^{1/2} = 0$, the bandgaps of BFO microspheres, microcubes and submicrometer-sized particles were calculated to be 2.05, 2.02 and 2.10 eV, respectively (Table 1), which are comparable to the values previously reported [5]. The optical absorption property suggests their potential applications as photocatalyst activated by visible light.

4 Conclusions

In the present work, micro- and submicrometer-sized BFO powders with different morphologies have been successfully synthesized by sol–gel–hydrothermal method at 200 °C for 24 h using KOH mineralizer. A possible formation mechanism of BFO microcrystals was proposed and the difference of the morphology between BFO microcrystals may be contributed to the changed crystal growth behavior caused by the varying OH^- concentration. Additionally, the UV–vis absorption of the BFO powder

indicates its promising prospect as visible light-driven photocatalyst.

Acknowledgments This work was financially supported by a project of Natural Science Foundation of Anhui Province (1108085J14), the National Natural Science Foundation of China (50972035), and a Program for New Century Excellent Talents in University, State Education Ministry (NCET-08-0766).

References

1. F. Kubel, H. Schmid, Acta Crystallogr. **B46**, 698 (1990)
2. G. Catalan, J.F. Scott, Adv. Mater. **21**, 2463 (2009)
3. J. Wang, J.B. Neaton, H. Zheng, V. Nagarajan, S.B. Ogale, B. Liu, D. Viehland, V. Vaithyanathan, D.G. Schlom, U.V. Waghmare, N.A. Spaldin, K.M. Rabe, M. Wuttig, R. Ramesh, Science **299**, 1719 (2003)
4. Y.P. Wang, L. Zhou, M.F. Zhang, X.Y. Chen, J.-M. Liu, Z.G. Liu, Appl. Phys. Lett. **84**, 1731 (2004)
5. F. Gao, X.Y. Chen, K.B. Yin, S. Dong, Z.F. Ren, F. Yuan, T. Yu, Z.G. Zou, J.M. Liu, Adv. Mater. **19**, 2889 (2007)
6. S. Li, Y.H. Lin, B.P. Zhang, J.F. Li, C.W. Nan, J. Appl. Phys. **105**, 054310 (2009)
7. F. Gao, Y. Yuan, K.F. Wang, X.Y. Chen, F. Chen, J.M. Liu, Z.F. Ren, Appl. Phys. Lett. **89**, 102506 (2006)
8. J. Wei, H.Y. Li, S.C. Mao, C. Zhang, Z. Xu, B. Dkhil, J. Mater. Sci.: Mater. Electron. (2012). doi:10.1007/s10854-012-0676-y
9. Z.K. Liu, Y.J. Qi, C.J. Lu, J. Mater. Sci.: Mater. Electron. **21**, 380 (2010)
10. N. Das, R. Majumdar, A. Sen, H.S. Maiti, Mater. Lett. **61**, 2100 (2007)
11. S. Ghosh, S. Dasgupta, A. Sen, H.S. Maiti, Mater. Res. Bull. **40**, 2073 (2005)
12. M. Popa, D. Crespo, J.M. Calderon-Moreno, S. Preda, V. Fruth, J. Am. Ceram. Soc. **90**, 2723 (2007)
13. S.M. Selbach, M.-A. Einarsrud, T. Tybell, T. Grande, J. Am. Ceram. Soc. **90**, 3430 (2007)
14. J.H. Xu, H. Ke, D.C. Jia, W. Wang, Y. Zhou, J. Alloys Compd. **472**, 473 (2009)
15. T. Liu, Y.B. Xu, S.S. Feng, J.Y. Zhao, J. Am. Ceram. Soc. **94**, 3060 (2011)
16. J.T. Han, Y.H. Huang, X.J. Wu, C.L. Wu, W. Wei, B. Peng, W. Huang, J.B. Goodenough, Adv. Mater. **18**, 2145 (2006)
17. C. Chen, J.R. Cheng, S.W. Yu, L.J. Che, Z.Y. Meng, J. Cryst. Growth **291**, 135 (2006)
18. Y.G. Wang, G. Xu, Z.H. Ren, X. Wei, W.J. Weng, P.Y. Du, G. Shen, G.R. Han, J. Am. Ceram. Soc. **90**, 2615 (2007)
19. C.M. Cho, J.H. Noh, I.-S. Cho, J.-S. An, K.S. Hong, J.Y. Kim, J. Am. Ceram. Soc. **91**, 3753 (2008)
20. A. Gajovic, S. Sturm, B. Jancar, A. Santic, K. Zagar, M. Ceh, J. Am. Ceram. Soc. **93**, 3173 (2010)
21. B. Liu, B.B. Hu, Z.L. Du, Chem. Commun. **47**, 8166 (2011)
22. X.M. Lu, J.M. Xie, Y.Z. Song, J.M. Lin, J. Mater. Sci. **42**, 6824 (2007)
23. S. Li, Y.H. Lin, B.P. Zhang, Y. Wang, C.W. Nan, J. Phys. Chem. C **114**, 2903 (2010)
24. X.Z. Chen, Z.C. Qiu, J.P. Zhou, G.Q. Zhu, X.B. Bian, P. Liu, Mater. Chem. Phys. **126**, 560 (2011)
25. Y.G. Wang, G. Xu, L.L. Yang, Z.H. Ren, X. Wei, W.J. Weng, P.Y. Du, G. Shen, G.R. Han, Ceram. Int. **35**, 1285 (2009)
26. L. Zhang, X.F. Cao, Y.L. Ma, X.T. Chen, Z.L. Xue, J. Solid State Chem. **183**, 1761 (2010)
27. L.F. Fei, J.K. Yuan, Y.M. Hu, C.Z. Wu, J.L. Wang, Y. Wang, Cryst. Growth Des. **11**, 1049 (2011)
28. T.-J. Park, G.C. Papaefthymiou, A.J. Viescas, A.R. Moodenbaugh, S.S. Wong, Nano Lett. **7**, 766 (2007)
29. T. Liu, Y.B. Xu, J.Y. Zhao, J. Am. Ceram. Soc. **93**, 3637 (2010)
30. X.L. Chen, Y. Tang, L. Fang, H. Zhang, C.Z. Hu, H.F. Zhou, J. Mater. Sci.: Mater. Electron. (2012). doi:10.1007/s10854-011-0617-1
31. J.B. Liu, H. Wang, Y.D. Hou, M.K. Zhu, H. Yan, Y. Masahiro, Nanotechnology **15**, 777 (2004)
32. L. Hou, Y.D. Hou, X.M. Song, M.K. Zhu, H. Wang, H. Yan, Mater. Res. Bull. **41**, 1330 (2006)
33. Y.D. Hou, L. Hou, T.T. Zhang, M.K. Zhu, H. Wang, H. Yan, J. Am. Ceram. Soc. **90**, 1738 (2007)
34. Y.D. Hou, L. Hou, M.K. Zhu, H. Yan, Appl. Phys. Lett. **89**, 243114 (2006)
35. Z.Q. Song, S.B. Wang, W. Yang, M. Li, H. Wang, H. Yan, Mater. Sci. Eng. B **113**, 121 (2004)
36. G.Z. Wang, R. Sæterli, P.M. Rørvik, A.T.J. van Helvoort, R. Holmestad, T. Grande, M.-A. Einarsrud, Chem. Mater. **19**, 2213 (2007)
37. W.G. Lu, J.Y. Fang, Y. Ding, Z.L. Wang, J. Phys. Chem. B **109**, 19219 (2005)
38. Y.Y. Xu, D.R. Chen, X.L. Jiao, J. Phys. Chem. B **109**, 13561 (2005)
39. U.A. Joshi, J. Jum Suk, P.H. Borse, L. Jae Sung, Appl. Phys. Lett. **92**, 242106 (2008)
40. Y.N. Huo, Y. Jin, Y. Zhang, J. Mol. Catal. A: Chem. **331**, 15 (2010)
41. P. Kubelka, F. Munk, Z. Tech. Phys. **12**, 593 (1931)
42. Y.P. He, Y.M. Miao, C.R. Li, S.Q. Wang, L. Cao, S.S. Xie, G.Z. Yang, B.S. Zou, C. Burda, Phys. Rev. B **71**, 125411 (2005)
43. A. Jaiswal, R. Das, K. Vivekanand, P. Mary Abraham, S. Adyanthaya, P. Poddar, J. Phys. Chem. C **114**, 2108 (2010)
44. Y.I. Kim, S.J. Atherton, E.S. Brigham, T.E. Mallouk, J. Phys. Chem. **97**, 11802 (1993)